Biosensors and Bioelectronics 280 (2025) 117444

Contents lists available at ScienceDirect

Biosensors and Bioelectronics

journal homepage: www.elsevier.com/locate/bios

$BiVO_4/C_3N_4$ heterojunction-gated organic photoelectrochemical transistor for sensitive detection of neurotransmitter

Ting Cai [a,1], Wenran Zhang [a,1], Francessca Charlton [b], Yali Sun [a], Yuxuan Chen [a],
Ying Fu [b,*], Qian Zhang [a,**], Shenghua Liu [a,***]

[a] School of Materials, Shenzhen Campus of Sun Yat-sen University, Shenzhen, Guangdong, 518107, PR China
[b] Department of Pure and Applied Chemistry, University of Strathclyde, Glasgow, United Kingdom

ARTICLE INFO

Keywords:
$BiVO_4/C_3N_4$
Organic photoelectrochemical transistor
Neurotransmitter
Dopamine
Photoelectrochemical biosensing

ABSTRACT

Developing advanced signal amplification strategies is essential for improving performance of state-of-the-art photoelectrochemical (PEC) analysis and integrated organic electrochemical transistor (OECT) devices. This study introduces a novel approach by integrating a $BiVO_4/C_3N_4$ heterojunction photoanode with organic photoelectrochemical transistor (OPECT) devices to achieve efficient signal modulation. The $BiVO_4/C_3N_4$ heterojunction is designed to promote effective charge separation and enhance the photoelectrochemical effect, introducing an efficient dual electrochemical signal amplification strategy. Dopamine (DA), a key neurotransmitter, is used as the target analyte as a proof-of-concept study. It acts as an effective electron donor, directly participating in redox reactions to amplify the channel signal and indirectly modulating the channel response through the $BiVO_4/C_3N_4$ electrode. The signal amplification results in the signal enhancement of three orders of magnitude. The developed bioanalytical method enables sensitive detection of DA with a good linear range from 10^{-7} to 10^{-4} M. Importantly, this dual amplification mechanism is independent of interactions between biological recognition molecules and analytes, providing a universal dual electrochemical signal amplification OPECT sensing platform. These findings indicate the potential this device has for the real-time monitoring of neurotransmitter levels, important for neurological disease monitoring.

1. Introduction

Photoelectrochemical (PEC) biosensing, based upon photon-to-electron conversion utilising semiconductor materials has garnered significant attention as an analytical technique due to its low background signal, ease of fabrication, and rapid response. (Li et al., 2024; Tan et al., 2023; Wang et al., 2019; Zhang et al., 2019; Zhou et al., 2021). Traditional PEC sensing is limited however due to its inherent inability to amplify signals (Zhao et al., 2015). Organic electrochemical transistors (OECTs) are bioelectronic devices characterised by high carrier mobility, high transconductance, low cost, and ease of miniaturisation. These devices can significantly amplify small changes in interfacial potential, generating channel currents as output signals (Ban et al., 2023; Braendlein et al., 2017; Ji et al., 2020; Koklu et al., 2022; Rivnay et al., 2018; Song et al., 2023; Tan et al., 2021; Almulla et al., 2024). We have previously used OECTs to construct a portable monitoring platform for analysing microRNA expression levels at different stages of cancer (Fu et al., 2021). A problem observed with traditional OECT biosensors however is the external voltage applied to the gate electrode, which not only hinders integration and consumes energy, but may also affect the biological activity of some fragile molecules (Rivnay et al., 2013). The newly emerged organic photoelectrochemical transistor (OPECT) comprises a photosensitive gate electrode, source, and drain, endowing traditional OECTs with light-collecting capabilities. Any slight changes in the photo-induced voltage (V_P) under light stimulation can effectively modulate the doping/de-doping state of the poly (3,4-ethylene dioxythiophene):poly (styrene sulfonate) (PEDOT:PSS) channel (Hu et al., 2024). OPECTs have been used for the detection of a range of biomarkers including proteins, DNA, and enzymes (Ban et al., 2022; Gao et al., 2022; Hu et al., 2022; Lu et al., 2022; Song et al., 2018;

---

* Corresponding author.
** Corresponding author.
*** Corresponding author.
E-mail addresses: ying.fu@strath.ac.uk (Y. Fu), zhangqian6@mail.sysu.edu.cn (Q. Zhang), liushengh@mail.sysu.edu.cn (S. Liu).
[1] The authors contributed equally.

https://doi.org/10.1016/j.bios.2025.117444
Received 21 October 2024; Received in revised form 29 March 2025; Accepted 2 April 2025

Xu et al., 2022; Zhang et al., 2024; Zhu et al., 2023). Utilisation of OPECTs for neurotransmitter detection however is less commonly reported.

Neurotransmitters are chemical compounds released by nerve cells for signal transmission within the central nervous system (Cai et al., 2015; Costa and Schoenbaum, 2022). Abnormal neurotransmitter levels can cause intractable diseases involving descending/ascending modulatory pathways or organ dysfunction. Methods for neurotransmitter level detection provides promising tools in the diagnosis of brain diseases such as Parkinson's disease (Cramb et al., 2023; Fang et al., 2018; Lambert et al., 1995; Lu et al., 2020). Dopamine (DA, 3,4-dihydroxyphenylalanine) is one of the most important neurotransmitters in the mammalian central nervous system, and monitoring its expression level within the body can be used for early diagnosis of neurological disorders and treatment monitoring (Gowrishankar et al., 2014; Soliman et al., 2018).

The challenge of using OPECTs in neurotransmitter detection may lie in photosensitive gate modification to achieve the effective separation of input (light) and output (electric) signals, resulting in operation at zero bias voltage with the decreased background noise. Bismuth vanadate ($BiVO_4$), a typical Bi-based photosensitive material, has been widely used in PEC as a visible light response material (Wang et al., 2018a, 2018b; Yuan et al., 2024). However, $BiVO_4$ has low photogenerated electron yield due to its low carrier mobility and short hole diffusion distance. One of the promising methods to improve performance is to form heterojunctions at the interface of $BiVO_4$ to improve the separation efficiency of carriers due to the cascaded energy levels, which leads to an internal electric field. Graphite carbon nitride (C_3N_4) is a two-dimensional semiconductor photocatalyst with adjustable bandgaps, which has high thermal and chemical stability, owing to its lamellar structure. Therefore, the $BiVO_4/C_3N_4$ heterostructures are expected to significantly improve the electron-hole pairs separation and the interfacial charge transfer efficiency in OPECTs (Feng et al., 2017; Ye et al., 2019).

Using light as the sole operation trigger, we herein report a highly sensitive OPECT for DA detection based on PEDOT:PSS with mixed ion/electron conductivity (OMIEC), and $BiVO_4/C_3N_4$ as the photoactive material. The constructed ultrasensitive monitoring platform, based upon an OECT employs a $BiVO_4/C_3N_4$ binary system as the photogating material. The sheet-structured C_3N_4 enhances the photogating effect due to the suppression of charge recombination of electron-hole pairs at the heterojunction. Subsequent to illumination, an abundance of holes is generated in the valence band of C_3N_4. These holes oxidise DA, the faradaic current generated from which acts as an effective electron donor increasing the potential drop across the electrolyte/gate interface, driving cations into the PEDOT:PSS channel. Additionally, the enhanced electron-hole separation efficiency at the $BiVO_4/C_3N_4$ electrode due to DA increases the effective gate voltage of the transistor, thereby indirectly modulating the drain current (I_{DS}). This dual electrochemical signal amplification mechanism is therefore independent of specific interactions between biological recognition molecules and analytes, yielding a sensitive OPECT response for DA detection.

As shown in Fig. 1a, bismuth precursor films (BPFs) were formed on fluorine-doped SnO_2 (FTO) glass substrates using the electrodeposition method. After calcination with vanadyl acetylacetonate and removal of excess V_2O_5, transparent yellow films were obtained. After impregnation, $BiVO_4/C_3N_4$ heterojunction was formed as the photoactive gate. DA participates in the electron transfer on the $BiVO_4/C_3N_4$ modified gate electrode surface, suppressing the charge recombination of electron-hole pairs and enhancing the photocurrent response, thereby outputting in the form of reduced I_{DS}.

2. Material and methods

2.1. Experimental section

Reagents and Apparatus: Poly (3,4ethylenedioxythiophene):poly (styrenesulfonate) (PEDOT:PSS, Clevios PH1000) was purchased from Xian Yuri Solar Co, Ltd, dimethyl sulfoxide (DMSO), $Bi(NO_3)_3•5H_2O$, acetic acid, HNO_3, and 3-glycidoxypropyltrimethoxysilane (GOPS) were purchased from Sigma-Aldrich. Melamine, D^+glucose (GLU), lactic acid (LA), uric acid (UA) and dopamine (DA) were obtained from Aladdin Reagent Company. 0.1 M potassium phosphate buffer (PBS) buffer was obtained from biosharp.

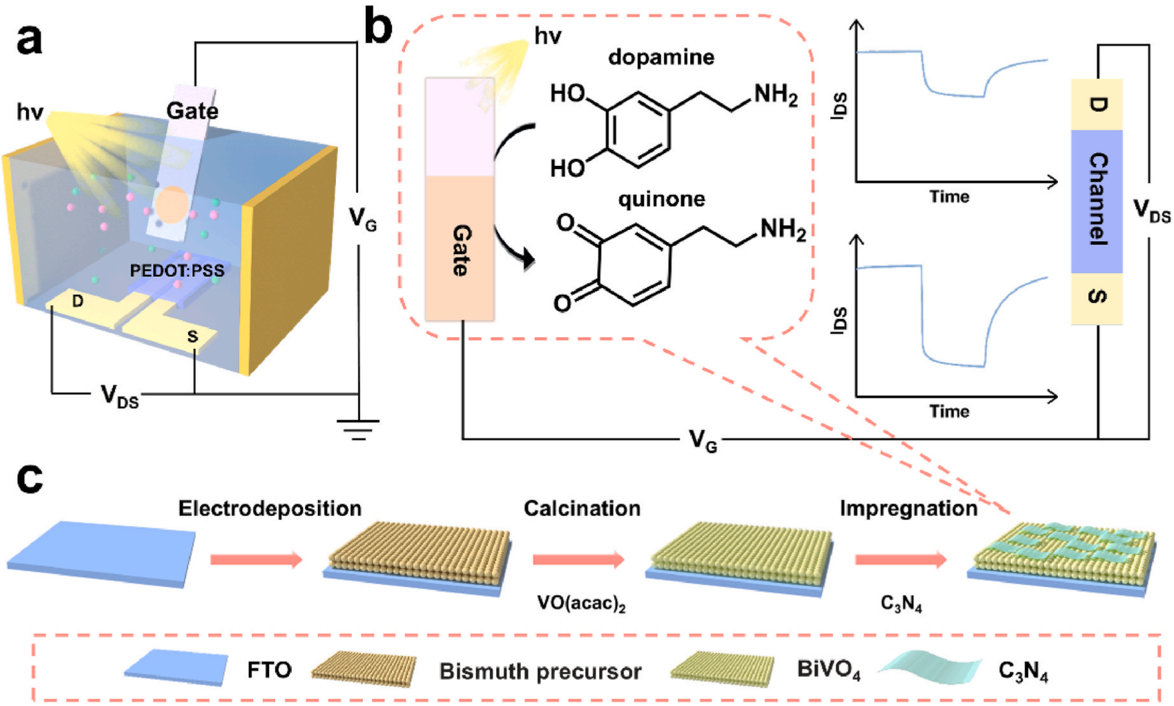

Fig. 1. Schematic diagram of the $BiVO_4/C_3N_4$-gated OPECT system. (a) The structure of the OPECT system is based on the gating effect of $BiVO_4/C_3N_4$. (b) The biosensing mechanism of the OPECT system for DA and the corresponding changes in I_{DS}. (c) The synthetic process of $BiVO_4/C_3N_4$.

Fabrication of OECT devices: The device fabrication parameters are based on our previous work (Cai et al., 2024). The glass substrate with the size of 1.5 cm × 1.5 cm was sonicated in deionised (DI) water, ethanol, isopropanol, and acetone for 15 min each, followed by ozone plasma treatment. Titanium (10 nm) and gold (100 nm) were sequentially sputtered onto the glass substrate to form the channel with a length of 0.2 mm and a width of 6.0 mm. The PEDOT:PSS film was spin-coated on the glass substrate at 3000 rpm using the PEDOT:PSS solution containing 5.0 % v/v dimethyl sulfoxide (DMSO) and 1.0 % v/v (3-glycidyloxypropyl)trimethoxysilane (GOPS). Finally, the sample was heated to 180 °C in an argon atmosphere for 60 min in a glovebox.

Preparation of $BiVO_4$ electrode: 0.2 M bismuth precursor solution was prepared by dissolving 8 mmol of $Bi(NO_3)_3{\bullet}5H_2O$ in 40 mL aqueous solution containing 16 mL of acetic acid and 1.6 mL of concentrated HNO_3. Electrodeposition in this solution was performed on FTO glass substrates using a three-electrode cell with a Pt counter electrode and a saturated Ag/AgCl reference electrode. The external bias was maintained at 2.82 V vs. reversible hydrogen electrode for 1.5 h. The obtained bismuth precursor films were rinsed with DI water and dried naturally at room temperature. To convert the bismuth precursor films to $BiVO_4$ films, 80 μL of vanadyl acetylacetonate solution (0.05 M in acetyl acetone) was dropped uniformly on the bismuth precursor films. After drying at 100 °C on a hot plate, the films were annealed at 500 °C for 2 h in air. The as-annealed films were then immersed in a 1 M NaOH solution for 20 min with mild stirring to remove the excessive V_2O_5. Finally, the films were rinsed with DI water and dried in an oven at 60 °C.

Preparation of C_3N_4: The bulk graphite-C_3N_4 was fabricated by directly heating low-cost melamine. In detail, 5 g melamine powder was placed in an alumina crucible with a cover, then heated to 500 °C for 2 h in a muffle furnace with a heating rate of 2 °C min^{-1}. The obtained bulk C_3N_4 was ground into small powder, and 100 mg C_3N_4 powder was dispersed in 100 mL isopropyl alcohol and exfoliated by ultrasonication for 24 h to obtain C_3N_4 sheets (C_3N_4-NS). The resultant dispersion was centrifuged at 3000 rpm for 10 min, and the supernatant containing exfoliated C_3N_4-NS was collected by pipette.

Preparation of $BiVO_4/C_3N_4$: The $BiVO_4$ photoanodes were immersed into 15 mL C_3N_4-NS supernatants for 1 h. After being rinsed with DI water, the obtained $BiVO_4/C_3N_4$ photoanodes were annealed at 350 °C in air for 1 h for combination.

OPECT and PEC Measurements: OPECT characterisation was conducted using a source meter (KEYSIGHT B2902B) equipped with a xenon lamp (CEL-PE300L-3 A) with illumination intensity equivalent to standard solar irradiance. The test parameters are: the transfer characteristics (I_{DS}-V_G) were measured at a constant drain voltage of $V_{DS} = 0.1$ V, and the I_{DS}-t curves were tested under a gate voltage of 0 V (Huang et al., 2023). Mott-Schottky (MS) measurements were performed in a 0.1 M PBS electrolyte using a conventional three-electrode system, where the composite-coated FTO electrode, Ag/AgCl electrode, and Pt electrode were used as the working electrode, reference electrode, and counter electrode, respectively.

2.1.1. Characterisation

The morphologies and crystal structures of the films were characterised by scanning electron microscopy (SEM) (JSM-IT500, JEOL and GeminiSEM 300, ZEISS), and X-ray diffraction (XRD) (D8 Advance, Bruker) with Cu Kα (λ = 0.15418 nm) radiation, respectively. UV–vis absorption spectra of the films were performed on a Thermo Evolution 201 spectrophotometer. PEC performance of the obtained photoanode was conducted using a typical three-electrode cell (Pt as CE, Ag/AgCl as RE) with a Xe 300 W lamp as the coupled light source. 0.5 M PBS (pH 7) was used as the electrolyte for all PEC measurements (Fig. S1). Electrochemical impedance spectra were collected with an AC voltage amplitude of 10 mV at the open circuit potentials of the films under 3 sun illumination in the frequency range of 0.01 Hz–100 kHz.

3. Results and discussion

3.1. Light-sensitive gate based on $BiVO_4/C_3N_4$ heterostructures

To fabricate high-performing $BiVO_4$ photoanode thin films, bismuth precursor films were grown via electrodeposition on FTO glass substrates in a three-electrode cell with an aqueous solution containing Bi (III) ions. Calcination of the substrates was then performed in vanadyl acetylacetonate. As shown in Fig. 2a, XRD confirms that no impurities are formed in the $BiVO_4$ films as only monoclinic $BiVO_4$ and FTO peaks are observed. In Fig. S2, SEM images show that the $BiVO_4$ films are composed of adjoining grains ranging from 200 to 500 nm. The uniform and well-distributed $BiVO_4$ crystals can be observed with no obvious pores in the film. As shown in Fig. 2b, the flaky C_3N_4 has been successfully grown on $BiVO_4$. In addition, as the light absorption property is a significant element in evaluating the PEC activity of photoanodes, ultraviolet–visible spectroscopy (UV–vis) absorption spectra of samples were examined (Fig. 2c). It proves that the addition of C_3N_4 into $BiVO_4$ can improve the capability of $BiVO_4$ for harvesting visible light for high PEC performance, presenting the semi-transparent yellow films (inset of Fig. 2c). Fig. S3 shows the corresponding Tauc diagram of $BiVO_4$, and the band gaps of $BiVO_4$ are 2.58 eV.

The transient photocurrent responses of the samples were recorded under zero V_G and visible light irradiation. As depicted in Fig. 3a, the $BiVO_4$ and $BiVO_4/C_3N_4$ samples exhibit photocurrent densities of 5 μA and 15 μA, respectively. The multi-cycle switching stability tests are shown in Fig. S4. This increase in photocurrent density indicates improved separation efficiency of photoinduced charge carriers due to the formation of a p-n heterojunction between $BiVO_4$ and C_3N_4.

Upon the addition of DA, the $BiVO_4/C_3N_4$/DA composite demonstrates a significant increase in photocurrent density, reaching as high as 45 μA, which is 2.4 and 4.1 times higher than those of $BiVO_4$ and $BiVO_4/C_3N_4$, respectively. This phenomenon is ascribed to the oxidation of DA by the abundant holes generated in the valence band (VB) of C_3N_4, which can effectively suppress the rapid recombination of the photogenerated electron-hole pairs (Çakar et al., 2022). The enhanced photoelectrochemical (PEC) response of the $BiVO_4/C_3N_4$ composite and further enhanced response to DA therefore provides a foundational basis for the DA sensor. Electrochemical impedance spectroscopy (EIS) was carried out to study the interfacial electron transfer rate of the photosensitive gate electrode, as shown in Fig. 3b. Based on the Randles circuit fitting of the Nyquist plots, we calculated the charge transfer resistance (R_{ct}) of $BiVO_4$ (487 KΩ), $BiVO_4/C_3N_4$ (191 KΩ), and $BiVO_4/C_3N_4$/DA (16 KΩ). The R_{ct} of $BiVO_4/C_3N_4$/DA is smaller than that of $BiVO_4$ and $BiVO_4/C_3N_4$, indicating the facilitated transfer of photogenerated electrons and a potentially increased PEC response. This reduction in R_{ct} suggests enhanced charge separation and efficient electron transport, contributing to improved photoelectrochemical performance.

To investigate the heterojunction formed between $BiVO_4$ and C_3N_4, Mott-Schottky (MS) curves (Fig. S5) were measured to calculate Tauc plots of $BiVO_4$. In MS curves, $BiVO_4$ exhibits a positive slope, indicating that $BiVO_4$ is an n-type semiconductor. Due to the fact that the conduction bands (CB) of n-type semiconductors are 0.1–0.3 V lower than the flat-band potential (Efb), $BiVO_4$'s CB was estimated to be 0.08 V vs RHE. Tauc plots revealed that the energy band-gap values of $BiVO_4$ was 2.58 eV. We referred to other literature (Ye et al., 2019). for the bandgap and conduction band position of C_3N_4, which are 2.41 eV and −0.53 V, respectively.

The photoelectrochemical sensing mechanism for DA in the designed composite electrode system is illustrated in Fig. 3c. $BiVO_4$ and C_3N_4 form a typical type II heterojunction. Driven by the electric field in the p-n junction, holes migrate from the VB of $BiVO_4$ to the VB of C_3N_4. Due to the electric field in the heterojunction, photogenerated electrons are transferred from the CB of C_3N_4 to the CB of $BiVO_4$. Consequently, the electron-hole separation efficiency and photoelectric performance are

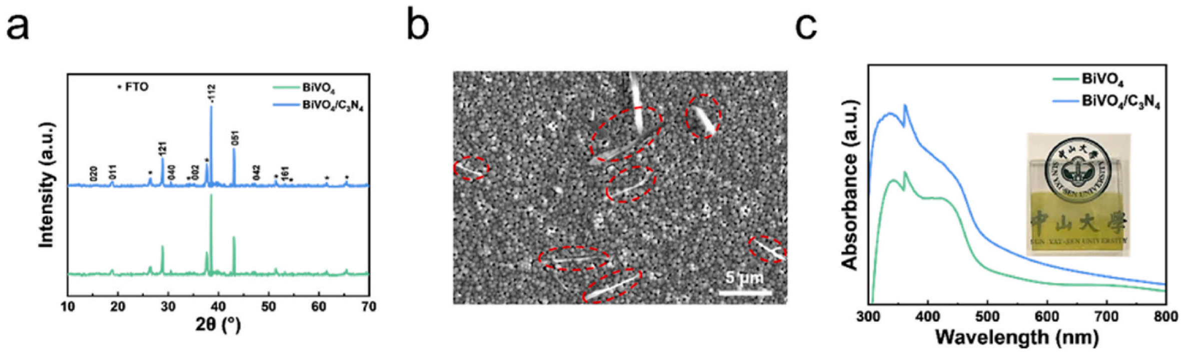

Fig. 2. (a) XRD patterns of $BiVO_4$ and $BiVO_4/C_3N_4$. (b) SEM images of $BiVO_4/C_3N_4$. The red circles indicate the C_3N_4 nanosheet on $BiVO_4$.(c) UV–vis absorption spectra of $BiVO_4$ (green curve) and $BiVO_4/C_3N_4$ (blue curve), Inset: the image of the $BiVO_4/C_3N_4$ on FTO/Glass substrate. (For interpretation of the references to colour in this figure legend, the reader is referred to the Web version of this article.)

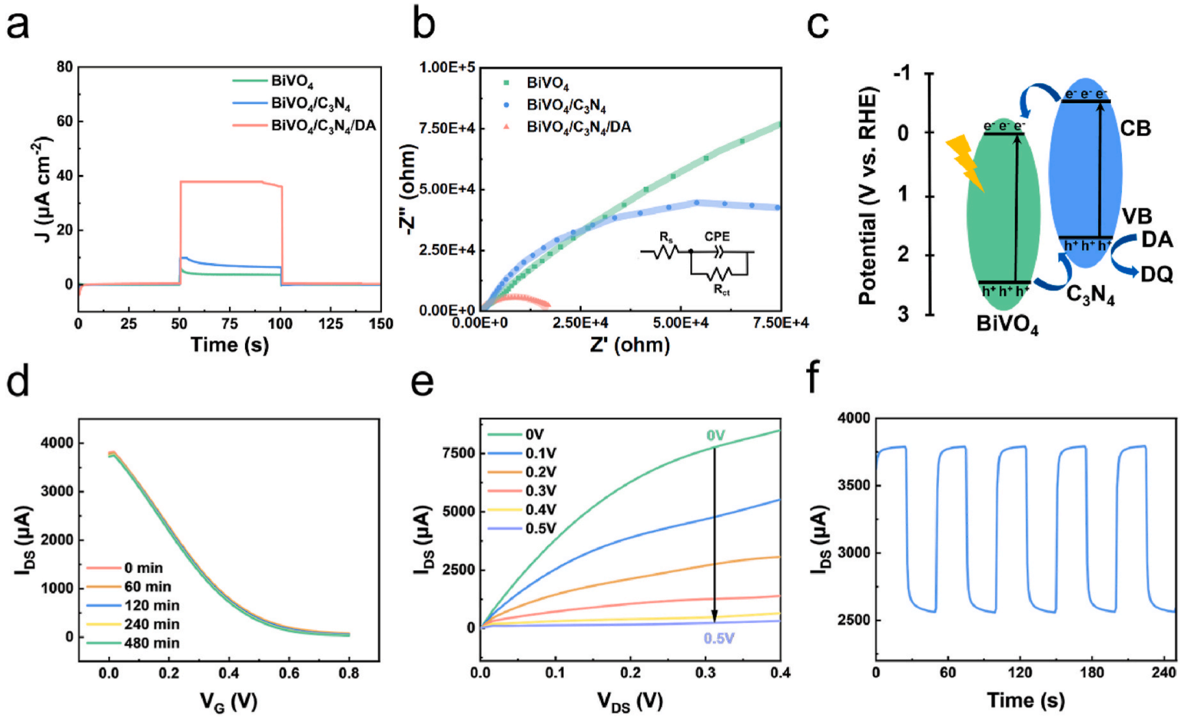

Fig. 3. (a) Photocurrent responses of $BiVO_4$ and $BiVO_4/C_3N_4$ in 0.1 M PBS electrolyte containing 10^{-3} M DA for one light off/on/off cycle. (b) EIS Nyquist plots of different electrodes, insert shows the Randles Circuit used for the EIS analysis. (c) The photoexcited charge transfer route within the type-II $BiVO_4/C_3N_4$ heterojunction with DA. (d) The transfer curves of the OECT device with an Ag/AgCl gate measured in PBS solution for up to 480 min. (e) The output curves of the OECT device with V_G ranging from 0 V to 0.5 V. (f) Transient I_{DS} response measured under square wave voltage V_G of 0.3 V.

significantly enhanced. Thus under visible light excitation, an abundance of holes are generated in the VB of C_3N_4. When DA is further added to the $BiVO_4/C_3N_4$ electrode under visible light excitation, the DA becomes oxidized by these holes forming dopamine o-quinone (DQ), participating in the electron transfer on the electrode surface. The released electrons are transferred to the valence band of C_3N_4 on the electrode surface and then to the conduction band of $BiVO_4$. Therefore, the photoelectric response is effectively enhanced, and the photo-gating effect is improved. The performance of the fabricated OECT with a PEDOT:PSS channel was evaluated using Ag/AgCl as the gate electrode. As shown in Fig. 3d, under a constant drain-source voltage (V_{DS}) of 0.1 V, when the gate voltage (V_G) was scanned from 0 to 0.8 V, the drain current (I_{DS}) significantly decreased from 3780 μA to 76 μA, demonstrating excellent gate control over the channel current. The corresponding transconductance curves are shown in Fig. S6. The nearly overlapping transfer characteristic curves further confirmed the superior stability of the device. The output curvesin Fig. 3e indicate that I_{DS} increased and reached saturation with the applied V_{DS} ranging from 0 to 0.4 V. A decrease in I_{DS} was observed with the applied V_G ranging from 0 V to 0.5 V, reflecting the modulation effect of the V_G on I_{DS}. Additionally, transient I_{DS} responses of the device were tested under a constant V_{DS} of 0.1 V with V_G pulses of 0.3 V (Fig. 3f). During multiple repetitive V_G on/off cycles, the I_{DS} values periodically decreased, indicating that V_G can effectively control the channel. The device demonstrated excellent operational stability, with a current retention rate of over 95 %.

3.2. *$BiVO_4/C_3N_4$ heterojuction-gated OPECT*

During OPECT operation, the fabricated $BiVO_4/C_3N_4$ photosensitive material was employed as the gate electrode in tracking the gate current I_{GS} and I_{DS} under visible light illumination at $V_G = 0$ V. As shown in

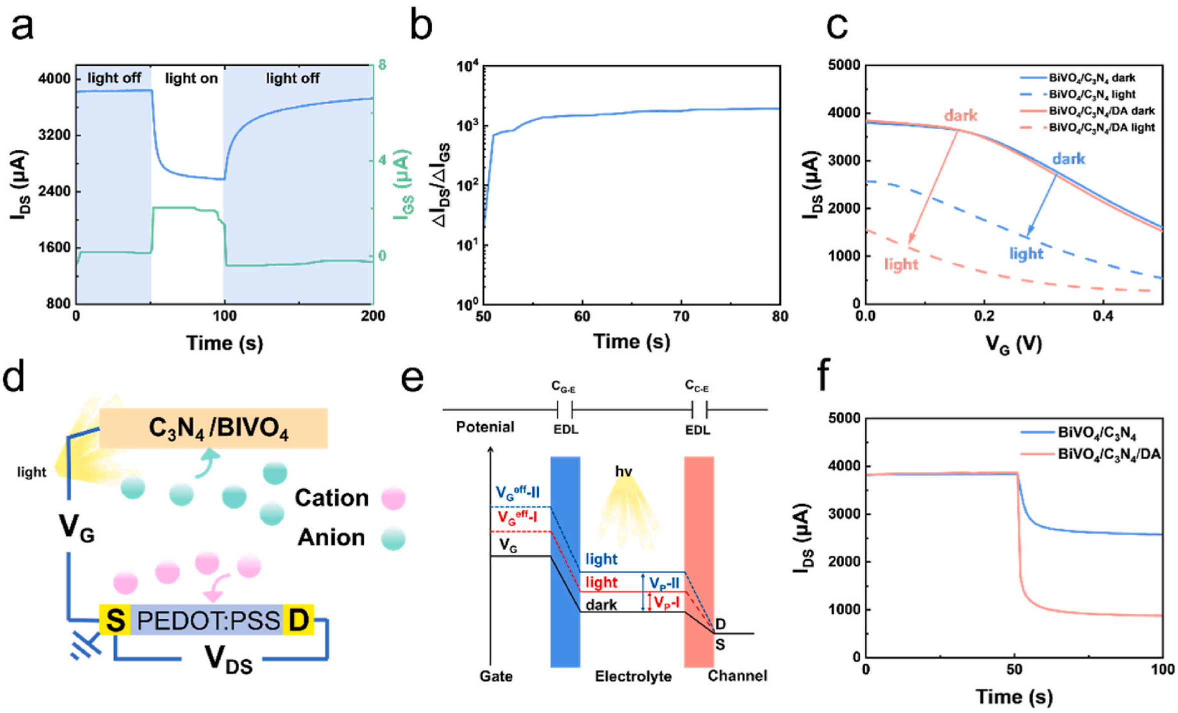

Fig. 4. (a) Transient I_{DS} (blue curve) and I_{GS} (green curve) responses of $BiVO_4/C_3N_4$ gate OPECT measured in 0.1 M PBS under zero gate bias and transient light illumination. (b) Corresponding calculated current gain. (c) Transfer characteristic curves of the OPECT system with the $BiVO_4/C_3N_4$ gate in the dark and light illumination with/without DA. (d) Illustration of the light-triggered ionic and charge transport in the OPECT device. (e) Potential distribution of the system. (f) Time-dependent I_{DS} variation in the OPECT biosensor. (For interpretation of the references to colour in this figure legend, the reader is referred to the Web version of this article.)

Fig. 4a, the I_{GS} generated by the photosensitive gate under dark conditions was negligible. While under illumination, I_{GS} (green curve) notably increased and stabilised at 2 μA and I_{DS} (blue curve) decreased from 3780 μA to 2580 μA. Notably, the minor change in I_{GS} induced by illumination resulted in a significant channel response of I_{DS}, indicating the excellent photo-gating capability of the constructed OPECT system. As depicted in Fig. 4b, the system achieved a current gain of $G = \Delta I_{DS}/\Delta I_{GS}$ up to 1000 times after illumination, achieving a three-order-of-magnitude amplification. Further investigation into the transfer characteristics of the $BiVO_4/C_3N_4$ gate electrode under light and dark conditions was conducted. As illustrated in Fig. 4c, $BiVO_4/C_3N_4$ (blue solid curve) and $BiVO_4/C_3N_4$/DA (red solid curve) exhibited nearly identical transfer curves with the absence of light illumination. However, after illumination, $BiVO_4/C_3N_4$/DA showed a more significant negative shift up to 60 %, compared to $BiVO_4/C_3N_4$, demonstrating that DA induced the enhancement of $BiVO_4/C_3N_4$ for more efficient channel de-doping in illuminated conditions. The corresponding photogating effect mechanism can be elucidated through the behaviour of photo-induced ion injection into the channel. The channel material PEDOT is a p-type semiconductor with holes as the charge carriers (Fig. 4d). Typically, the semiconductor is in an oxidized state with a high density of channel charge carriers. However, under illumination, the positive photovoltage generated by the n-type semiconductor drives cations into the semiconductor, leading to the reduction of $PEDOT^{+}$ to $PEDOT^{0}$ state, thereby reducing I_{DS} to a low value. Upon further introduction of DA, the enhanced positive Vp drives more cations into the channel, further decreasing the channel conductivity. This can be explained from the perspective of potential distribution, as depicted in Fig. 4e, where the gate and electrolyte, as well as the channel and electrolyte interfaces, can be equivalently represented as two series-connected capacitors ($C_{G\text{-}E}$ and $C_{C\text{-}E}$). The applied V_G falls across these two double layers. Under dark conditions, the potential drop across $C_{C\text{-}E}$ is $V_C=V_G/(1+\gamma)$, where $\gamma = C_{C\text{-}E}/C_{G\text{-}E}$ (Huang et al., 2023). Following illumination, the effective gate voltage becomes V_G^{eff}:

$$- \\ - V_G^{eff} \\ = V_G + (1+\gamma)V_P - \\ - - - - - - - - - - - - - - - \backslash \qquad (1)$$

The $V_{P\text{-}I}$ generated by $BiVO_4/C_3N_4$ without DA results in a higher V_G^{eff-I}, which enhances the potential drop across the channel, thereby increasing $V_G^{eff-I}/(1+\gamma)$. This ultimately leads to a higher doping level of PEDOT compared to $BiVO_4$. It is noteworthy that with the introduction of DA into the electrolyte, enhanced photovoltages $V_{P\text{-}II}$, and V_G^{eff-II} are generated, leading to further reduction in I_{DS}. Fig. 4f shows the $I_{DS\text{-}step}$ signal of the system at 0 V V_G before and after the addition of DA, corresponding to a concentration of 10^{-3} M DA. Upon exposure to light, the introduction of DA led to a significant increase in $I_{DS\text{-}step}$ from approximately 980 μA to around 2900 μA, which is consistent with the evolution of the transfer characteristics. The developed system can be effectively used for DA detection, as the change in I_{DS} is closely related to the oxidation of DA.

3.3. The modified OPECT for biosensing

The introduction of DA effectively enhances the PEC response of $BiVO_4/C_3N_4$ by modulating V_G, which in turn modifies and amplifies I_{DS}. Therefore, we constructed a biosensing platform for sensitive analysis of DA. Fig. 5a shows the I_{DS} response upon addition of different DA concentrations, where the ΔI value is defined as the difference in I_{DS} before and after illumination. The equation is as follows:

$$\Delta I = I_{Ds} - I_{Ds}^{*} \qquad (2)$$

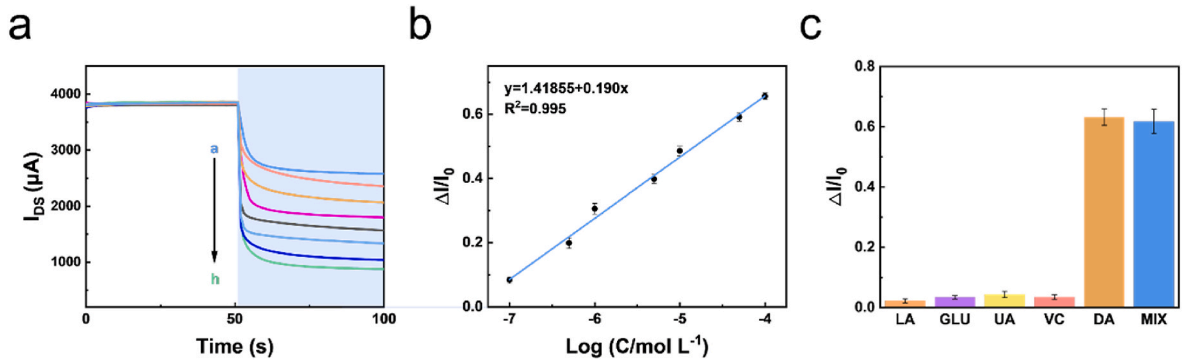

Fig. 5. (a) The time-dependent I_{DS} responses after illumination of $BiVO_4/C_3N_4$ gate OPECT at different DA concentrations (from top to bottom: 0, 10^{-7}, 5×10^{-6}, 10^{-6}, 5×10^{-5}, 10^{-5}, 5×10^{-5} and 10^{-4} M). (b) Corresponding calibration curve for determination of DA. RSD = 1.56 %–11.78 %. (c) Selectivity tests were conducted using DA, LA, UA, VC, and GLU at a concentration of 10^{-3} M. Error bars represent standard deviations from three independent experiments (n = 3).

I_{DS} and I^*_{DS} represent the channel current before and after illumination, respectively. The OPECT channel current response decreases with increasing DA concentration ranging from 10^{-7} to 10^{-4} M. Fig. 5b demonstrates a good linear relationship between $\Delta I/I_0$ value and the logarithm of DA concentration, with a regression equation of $\Delta I/I = 0.190 \log C + 1.41855$ ($R^2 = 0.995$). The limit of detection (LOD) is 10^{-7} mol/L, which is lower than the typical concentration range of DA found in human urine (0.3 μM–3 μM) (Sliesarenko et al., 2024), indicating the potential applicability and suitability of this method for analysing real samples. Furthermore, due to the combined enhanced PEC response and OECT channel current amplification, the developed biosensor exhibits a wider linear range and lower LOD compared to other electrochemical and PEC methods for DA analysis (Dashtian et al., 2021; Wang et al., 2022). Additionally, selectivity tests were conducted using lactic acid (LA), glucose (GLU), uric acid (UA), and vitamin C (VC), as well as their mixtures with DA. The selectivity of DA to potential interferents such as AA is likely due to the pH used for OPECTs. Shown in Fig. 5c, the $\Delta I/I_0$ for DA is significantly higher than other interfering substances, and the $\Delta I/I_0$ for the mixture is essentially the same as that for DA alone, indicating excellent selectivity of the biosensor.

4. Conclusion

A $BiVO_4/C_3N_4$ heterojunction-gated organic photoelectrochemical transistor (OPECT) was developed for the sensitive detection of DA. The $BiVO_4/C_3N_4$ heterostructure significantly improved the charge separation efficiency, leading to a three-order-of-magnitude amplification in the OPECT system. DA acts as an electron donor at the heterojunction-gated electrode, further amplifying the channel current and modulating the effective gate voltage. This dual-amplification DA detection mechanism is independent of bioreceptor modification and specific molecular interactions. A linear response range for DA from 10^{-7} M to 10^{-4} M was obtained with selectivity against multiple potential interfering substances. Our results show that the $BiVO_4/C_3N_4$-gated OPECT system is a promising advanced bioanalytical tool for sensitive and selective neurotransmitter detection, offering new opportunities for neurodegenerative disease monitoring. The use of the OPECT device for DA analysis in real samples will be investigated to further assess its suitability for clinical applications.

CRediT authorship contribution statement

Ting Cai: Writing – original draft, Validation, Supervision, Software, Methodology, Data curation, Conceptualization. **Wenran Zhang:** Visualization, Resources, Formal analysis, Conceptualization. **Francessca Charlton:** Writing – review & editing, Validation. **Yali Sun:** Visualization, Supervision. **Yuxuan Chen:** Visualization, Supervision. **Ying Fu:** Writing – review & editing, Validation, Supervision, Funding acquisition. **Qian Zhang:** Writing – review & editing, Software, Methodology, Funding acquisition. **Shenghua Liu:** Writing – review & editing, Visualization, Validation, Funding acquisition, Formal analysis, Conceptualization.

Declaration of competing interest

The authors declare that they have no known competing financial interests or personal relationships that could have appeared to influence the work reported in this paper.

Acknowledgements

This work was supported by Guangdong Innovative and Entrepreneurial Research Team Program (2021ZT09L227), Natural Science Foundation of Guangdong Province, China (2025A1515011790, 2022A1515010622), Open Research Fund of Songshan Lake Materials Laboratory (2023SLABFK06), Guangdong Youth Top Talent Program (2021QN02L119), Community for Analytical Measurement Science (CAMS) Fellowship and UKRI Tackling Infection Novel Technologies funding.

Appendix A. Supplementary data

Supplementary data to this article can be found online at https://doi.org/10.1016/j.bios.2025.117444.

Data availability

Data will be made available on request.

References

Almulla, L., Druet, V., Petoukhoff, C.E., Shan, W., Alshehri, N., Griggs, S., Wang, Y., Alsufyani, M., Yue, W., McCulloch, I., Laquai, F., Inal, S., 2024. Mater. Horiz. 11 (12), 2937–2949.
Ban, R., Li, C.-J., Xu, Y.-T., Zhu, Y.-Y., Ju, P., Li, Y.-M., Du, H.-J., Hu, J., Chen, G., Lin, P., Zhao, W.W., 2023. Anal. Chem. 95 (2), 1454–1460.
Ban, R., Lu, M.-J., Hu, J., Li, C.-J., Li, Y.-M., Gao, G., Wang, C.-S., Kong, F.-Y., Zhou, H., Lin, P., Zhao, W.-W., 2022. Biosens. Bioelectron. 218, 114752.
Braendlein, M., Lonjaret, T., Leleux, P., Badier, J.-M., Malliaras, G.G., 2017. Adv. Sci. 4 (1), 1600247.
Cai, Z., Rong, M., Zhao, T., Zhao, L., Wang, Y., Chen, X., 2015. J. Electroanal. Chem. 759, 32–37.
Cai, T., Zhang, W., Lian, L., Sun, Y., Xia, Z., Chen, Y., Shuai, J., Lin, P., Zhang, Q., Liu, S., 2024. Anal. Chem. 97 (1), 526–534.
Çakar, S., Çakıroğlu, B., Şen, Ş., Özacar, M., 2022. Microchem. J. 178, 107360.
Costa, K.M., Schoenbaum, G., 2022. Curr. Biol. 32 (15), R817–R824.
Cramb, K.M.L., Beccano-Kelly, D., Cragg, S.J., Wade-Martins, R., 2023. Brain 146 (8), 3117–3132.
Dashtian, K., Hajati, S., Ghaedi, M., 2021. Sens. Actuators, B 326, 128824.

Fang, J.-J., Yang, N.-N., Gao, E.-Q., 2018. Electrochem. Commun. 89, 32–37.

Feng, C., Wang, Z., Ma, Y., Zhang, Y., Wang, L., Bi, Y., 2017. Appl. Catal., B 205, 19–23.

Fu, Y., Wang, N., Yang, A., Xu, Z., Zhang, W., Liu, H., Law, H.K.-w., Yan, F., 2021. Anal. Chem. 93 (43), 14359–14364.

Gao, G., Hu, J., Li, Z., Xu, Q., Wang, C.-S., Jia, H.-M., Zhou, H., Lin, P., Zhao, W.-W., 2022. Biosens. Bioelectron. 209, 114224.

Gowrishankar, R., Hahn, M.K., Blakely, R.D., 2014. Neurochem. Int. 73, 42–48.

Hu, J., Jing, M., Huang, Y., Kou, B., Li, Z., Xu, Y., Yu, S., Zeng, X., Jiang, J., Lin, P., Zhao, W., 2024. Adv. Mater. 36 (38), 2405887.

Huang, Y.-T., Xu, K.-X., Liu, X.-S., Li, Z., Hu, J., Zhang, L., Zhu, Y.-C., Zhao, W.-W., Chen, H.-Y., Xu, J.-J., 2023. Anal. Chem. 95 (48), 17912–17919.

Hu, J., Lu, M.-J., Chen, F.-Z., Jia, H.-M., Zhou, H., Li, K., Zeng, X., Zhao, W.-W., Lin, P., 2022. Adv. Funct. Mater. 32 (26), 2109046.

Ji, W., Wu, D., Tang, W., Xi, X., Su, Y., Guo, X., Liu, R., 2020. Sens. Actuators, B 304, 127414.

Koklu, A., Wustoni, S., Guo, K., Silva, R., Salvigni, L., Hama, A., Diaz-Galicia, E., Moser, M., Marks, A., McCulloch, I., Grünberg, R., Arold, S.T., Inal, S., 2022. Adv. Mater. 34 (35), 2202972.

Lambert, G.W., Kaye, D.M., Lefkovits, J., Jennings, G.L., Turner, A.G., Cox, H.S., Esler, M. D.J.C., 1995. Circulation 92 (7), 1813–1818.

Li, G., Ren, H.-T., Liu, L., Shiu, B.-C., Lin, M.-C., Lou, C.-W., Li, T.-T., 2024. Mater. Res. Bull. 176, 112802.

Lu, M.-J., Li, C.-J., Ban, R., Chen, F.-Z., Hu, J., Gao, G., Zhou, H., Lin, P., Zhao, W.-W., 2022. ACS Sens. 7 (9), 2788–2794.

Lu, S., Hummel, M., Chen, K., Zhou, Y., Kang, S., Gu, Z., 2020. Electrochem. Commun. 114, 106715.

Rivnay, J., Inal, S., Salleo, A., Owens, R.M., Berggren, M., Malliaras, G.G., 2018. Nat. Rev. Mater. 3 (2), 17086.

Rivnay, J., Leleux, P., Sessolo, M., Khodagholy, D., Hervé, T., Fiocchi, M., Malliaras, G. G., 2013. Adv. Mater. 25 (48), 7010–7014.

Sliesarenko, V., Bren, U., Lobnik, A., 2024. Sens. Actuators. Rep. 7, 100199.

Soliman, A.M., Fathalla, A.M., Moustafa, A.A., 2018. Pharmacol. Rep. 70 (4), 661–667.

Song, J., Lin, P., Ruan, Y.-F., Zhao, W.-W., Wei, W., Hu, J., Ke, S., Zeng, X., Xu, J.-J., Chen, H.-Y., Ren, W., Yan, F., 2018. Adv. Healthcare Mater. 7 (19), 1800536.

Song, J., Liu, H., Zhao, Z., Lin, P., Yan, F., 2023. Adv. Mater. 36 (20), 2300034.

Tan, A.Y.S., Lo, N.W., Cheng, F., Zhang, M., Tan, M.T.T., Manickam, S., Muthoosamy, K., 2023. Biosens. Bioelectron. 219, 114811.

Tan, S.T.M., Giovannitti, A., Melianas, A., Moser, M., Cotts, B.L., Singh, D., McCulloch, I., Salleo, A., 2021. Adv. Funct. Mater. 31 (19), 2010868.

Wang, L., Zhu, W., Lu, W., Shi, L., Wang, R., Pang, R., Cao, Y., Wang, F., Xu, X., 2019. Biosens. Bioelectron. 142, 111577.

Wang, S., Chen, P., Bai, Y., Yun, J.-H., Liu, G., Wang, L., 2018a. Adv. Mater. 30 (20), 1800486.

Wang, Y., Tan, G., Liu, T., Su, Y., Ren, H., Zhang, X., Xia, A., Lv, L., Liu, Y., 2018b. Appl. Catal., B 234, 37–49.

Wang, Y., Wang, D., Dong, S., Qiao, J., Zeng, Z., Shao, S., 2022. Electrochim. Acta 414, 140207.

Xu, Y.-T., Li, Z., Yuan, C., Wu, J.-Q., Hu, J., Lin, P., Zhao, W.-W., Chen, H.-Y., Xu, J.-J., 2022. Adv. Opt. Mater. 10 (11), 2102687.

Ye, K.-H., Li, H., Huang, D., Xiao, S., Qiu, W., Li, M., Hu, Y., Mai, W., Ji, H., Yang, S., 2019. Nat. Commun. 10 (1), 3687.

Yuan, C., Xu, K.-X., Huang, Y.-T., Xu, J.-J., Zhao, W.-W., 2024. Adv. Mater. 36 (47), 2407654.

Zhang, M., Zhang, H., Zhou, Y., Yin, H., Yu, Z., Zhang, X., Ai, S., Wang, M., 2024. Anal. Chem. 96 (32), 13086–13095.

Zhang, X.Y., Liu, S.G., Zhang, W.J., Wang, X.H., Han, L., Ling, Y., Li, N.B., Luo, H.Q., 2019. Sens. Actuators, B 297, 126818.

Zhao, W.-W., Xu, J.-J., Chen, H.-Y., 2015. Chem. Soc. Rev. 44 (3), 729–741.

Zhou, Y., Yin, H., Ai, S., 2021. Coord. Chem. Rev. 447, 214156.

Zhu, Y., Ju, P., Wang, S., Jiang, T., Chi, J., Zhang, S., Zhai, X., Lu, Z., 2023. Anal. Chim. Acta 1240, 340757.